

Research Article

Inductorless Chua's Circuit: Experimental Time Series Analysis

R. M. Rubinger, A. W. M. Nascimento, L. F. Mello, C. P. L. Rubinger,
N. Manzanaraes Filho, and H. A. Albuquerque

Received 8 September 2006; Revised 6 November 2006; Accepted 11 February 2007

Recommended by José Manoel Balthazar

We have implemented an operational amplifier inductorless realization of the Chua's circuit. We have registered time series from its dynamical variables with the resistor R as the control parameter and varying from $1300\ \Omega$ to $2000\ \Omega$. Experimental time series at fixed R were used to reconstruct attractors by the delay vector technique. The flow attractors and their Poincaré maps considering parameters such as the Lyapunov spectrum, its sub-product the Kaplan-Yorke dimension, and the information dimension are also analyzed here. The results for a typical double scroll attractor indicate a chaotic behavior characterized by a positive Lyapunov exponent and with a Kaplan-Yorke dimension of 2.14. The occurrence of chaos was also investigated through numerical simulations of the Chua's circuit set of differential equations.

Copyright © 2007 R. M. Rubinger et al. This is an open access article distributed under the Creative Commons Attribution License, which permits unrestricted use, distribution, and reproduction in any medium, provided the original work is properly cited.

1. Introduction

Chaotic electronic circuits [1] have been widely studied during the last few decades due to their easy implementation, robustness, reproducibility of results, and also as a test platform for synchronization [2–4], chaos control [4–6], signal encryption [7], and secure communications [8, 9]. Also it is easy, through Kirchhoff's laws, to obtain the circuit described by a set of differential equations and carry on simulations which in most times, present good agreement with experimental data. The Chua's circuit [1, 10] is one of the most famous circuits on the literature and the reasons, among others, are:

- (1) Chua's circuit has a quite simple construction characterized by four passive linear elements and one of them with nonlinear $i(V)$ characteristic represented by a piecewise linear equation, as shown in Figure 1.1;

2 Mathematical Problems in Engineering

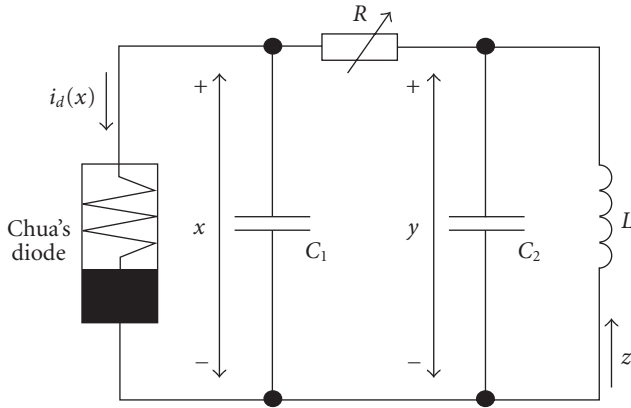


Figure 1.1. Chua's circuit. The dynamical variables are x , y , and z corresponding to the voltage across capacitor C_1 , the voltage across capacitor C_2 , and the current through the inductor, respectively. The nonlinear element is the Chua's diode and the nonlinearity is presented through $i_d(x)$ characteristics.

- (2) it exhibits a number of distinct routes to chaos and multistructural chaotic attractors [11];
- (3) attractors that occur in Chua's circuit arise from very complex homoclinic tangencies and loops of a saddle focus [11];
- (4) many opened questions on the system's behavior and the lack of a possibility to fully describe Chua's circuit from its equations [11].

The Chua's circuit has been the object of study of hundreds of papers, where its topological, numerical, physical, and dynamical characterizations are deeply investigated. See [12–15] and references therein.

Point (4) suggests that numerical analysis such as that carried on this work could provide some contributions to understand Chua's circuit dynamical behavior. Chua's circuit dynamical equations are given by

$$\begin{aligned}
 \frac{dx}{dt} &= f_1(x, y, z) = \left(\frac{y-x}{RC_1} \right) - \frac{i_d(x)}{C_1}, \\
 \frac{dy}{dt} &= f_2(x, y, z) = \left(\frac{x-y}{RC_2} \right) + \frac{z}{C_2}, \\
 \frac{dz}{dt} &= f_3(x, y, z) = -\frac{y}{L} - z \left(\frac{r_L}{L} \right), \\
 i_d(x) &= m_0 x + \frac{1}{2} (m_1 - m_0) \{ |x + B_p| - |x - B_p| \},
 \end{aligned} \tag{1.1}$$

where R, C_1, C_2 , and L are passive linear elements, r_L is the inductor's resistance, i_d is the current through Chua's diode with m_0, m_1 and B_p as parameters.

Chua's diode and the active component "inductor" were implemented according to Tórres and Aguirre [16]. This inductor implementation turns easy and compact to construct the Chua's circuit. It has another advantage since it can be designed as resistance free as have been carried on this work.

This paper is organized as follows: Section 2 is devoted to a detailed description of the parameters used to build and analyze Chua's circuit. A brief study of the equilibrium points of Chua's differential equations and the existence of a homoclinic loop is presented in Section 3. This was carried in order to identify the possible dynamical behavior for the chosen parameters of the circuit and to support the analyses carried in Section 4. In Section 4, we present the time series analysis of some illustrative experimental time series obtained from the Chua's circuit implementation. This section is the core of our work. Our aim is to characterize attractors obtained from this particular implementation of Chua's circuit with respect to its sensitivity to initial conditions and its dimension on the state space. Finally, concluding remarks are presented in Section 5.

2. Experimental details

Chua's circuit was constructed in a single face circuit board with the same scheme of [16] but with all capacitors 1000 times lower. This way $C_1 = 23.5 \text{ nF}$, $C_2 = 235 \text{ nF}$, and $L = 42.3 \text{ mH}$. These values were obtained from the combination of passive components and measured with a digital multimeter with a 3% precision. We evaluate the oscillation main frequency as a rough approximation by $1/(2\pi(LC_2)^{1/2})$ which gives about 1600 Hz. This oscillation frequency allowed us to store large time series for data analysis. Other parameters were experimentally determined. From Chua's diode $i(V)$ characteristics linear fittings as $B_p = 1.8 \text{ V}$, $m_1 = -0.758 \text{ mS}$, and $m_0 = -0.409 \text{ mS}$ with the significant digits limited by the fitting accuracy. Here S stands for inverse resistance unity. The resistor R , used as the control parameter, was a precision multiturn potentiometer and kept in the range of $1300 \text{ } \Omega$ to $2000 \text{ } \Omega$.

A data acquisition (DAQ) interface with 16 bit resolution, maximum sampling rate of 200 k samples/s, and adjustable voltage range of maximal peak voltage of 10 V was applied for data storage. The Chua's circuit oscillations were measured at the x point depicted in Figure 1.1 after passing through an active buffer. Also Labview[®] was used to develop data acquisition software and analysis [17, 18]. A Keithley 237 voltage/current source in series with the Chua's diode was applied to obtain the $i(V)$ data. For each time series the potentiometer R was detached from the circuit for resistance measurements with a $3(1/2)$ digit multimeter.

Four representative attractors obtained with R as $1480 \text{ } \Omega$, $1560 \text{ } \Omega$, $1670 \text{ } \Omega$, and $1792 \text{ } \Omega$ will be presented in Section 4 with the respective analyses. Particular attention will be given to the double scroll attractor.

3. Differential equation analysis

Considering a resistance free inductor, that is, $r_L = 0$, we have determined the operating points which coincide with the equilibrium points of (1.1), that is, its solution for

$$\dot{x} = \dot{y} = \dot{z} = 0. \quad (3.1)$$

4 Mathematical Problems in Engineering

Here the dot over the variables stands for time derivatives. The solutions correspond to the state space points $(-Ri_d(x), 0, i_d(x))$, which coincide with the interception of the load line with the graph of i_d in the plane $y = 0$. The load line is a straight line with slope $-1/R$ determined by the Kirchhoff's laws applied to the circuit composed by R and the Chua's diode. One of these equilibrium points will always be the origin $(0, 0, 0)$.

For

$$1300\Omega \leq R < -\frac{1}{m_1} \approx 1319.26\Omega, \quad (3.2)$$

(1.1) presents only the equilibrium point at the origin. The origin is a saddle focus point, since the Jacobian matrix of (1.1) at $(0, 0, 0)$ has one negative real eigenvalue and two complex eigenvalues with positive real parts. Here $f(x, y, z) = (f_1(x, y, z), f_2(x, y, z), f_3(x, y, z))$ is defined by (1.1). For $1318.93\Omega < R < 1319.26\Omega$, the origin is a (1-2)-saddle point, that is, the Jacobian matrix $Jf(0, 0, 0)$ has three real eigenvalues, being one negative and two positives.

For $R = 1319.26\Omega$, (1.1) presents a line segment of equilibrium points. In fact, all points $(x, 0, m_1x)$, $-B_p \leq x \leq B_p$, are equilibrium points of (1.1).

For

$$1319.26\Omega < R \leq 2000\Omega < -\frac{1}{m_0} \approx 2444.99\Omega, \quad (3.3)$$

(1.1) presents three equilibrium points

$$\begin{aligned} p_0 &= (0, 0, 0), \\ p_1 &= \left(\frac{R(m_0 - m_1)B_p}{Rm_0 + 1}, 0, \frac{(m_1 - m_0)B_p}{Rm_0 + 1} \right), \\ p_2 &= \left(\frac{R(m_1 - m_0)B_p}{Rm_0 + 1}, 0, \frac{(m_0 - m_1)B_p}{Rm_0 + 1} \right). \end{aligned} \quad (3.4)$$

For $1319.26\Omega < R < 1323.93\Omega$, p_0 is a (2-1)-saddle point, and for $1323.93\Omega \leq R \leq 2000\Omega$, the equilibrium point p_0 is of saddle-focus type, since the Jacobian matrix $Jf(p_0)$ has one real positive eigenvalue λ_{00} and two complex eigenvalues, λ_{01} and λ_{02} , with negative real parts. Therefore, p_0 has a 1-dimensional unstable manifold and a 2-dimensional stable manifold. The equilibrium points p_1 and p_2 are of saddle-focus type too, but their stable manifolds are 1-dimensional and their unstable manifolds are 2-dimensional, since the Jacobian matrix $Jf(p_1) = Jf(p_2)$ has one real negative eigenvalue and two complex eigenvalues with positive real parts.

The presence of homoclinic loops connecting p_0 to itself, that is, p_0 possesses a 2-dimensional stable manifold and a 1-dimensional unstable manifold which intersect non-transversely, for some value of the parameter R , plays a fundamental role in the existence of chaos in (1.1).

The existence of a homoclinic loop at p_0 is now outlined, according to [19]. Equation (1.1) can be written in dimensionless form

$$\begin{aligned}\frac{d\bar{x}}{d\tau} &= \alpha(\bar{x} - \bar{y}) + i(\bar{x}), \\ \frac{d\bar{y}}{d\tau} &= 0.1(\alpha(\bar{y} - \bar{x})) - \bar{z}, \\ \frac{d\bar{z}}{d\tau} &= 3.321\bar{y},\end{aligned}\tag{3.5}$$

where

$$i(\bar{x}) = \begin{cases} \bar{x} - 0.853 & \text{if } \bar{x} \leq -1 \text{ (region I),} \\ 1.853\bar{x} & \text{if } |\bar{x}| \leq 1 \text{ (region II),} \\ \bar{x} + 0.853 & \text{if } \bar{x} \geq 1 \text{ (region III),} \end{cases}\tag{3.6}$$

and the dimensionless variables and parameters are given by

$$\begin{aligned}\bar{x} &= \frac{1}{B_p}x, & \bar{y} &= \frac{1}{B_p}y, & \bar{z} &= \frac{1}{m_0B_p}z, \\ \tau &= \frac{m_0}{C_1}t, & i(\bar{x}) &= \frac{1}{m_0B_p}i_d(x), & \alpha &= \frac{1}{m_0R}.\end{aligned}\tag{3.7}$$

For $\alpha = -1.64042$ ($R = 1490.46\Omega$), (3.5) has the equilibrium points

$$\begin{aligned}q_0 &= (0, 0, 0), & q_1 &= (-1.33193, 0, -2.18493), \\ q_2 &= (1.33193, 0, 2.18493).\end{aligned}\tag{3.8}$$

The eigenvalues of the Jacobian matrix of (3.5) at q_0 are 0.406522 and $-0.178994 \pm i0.376325$, with the respective eigenvectors

$$\begin{aligned}e_0 &= (0.716695, 0.0847343, 0.69222), \\ f_0 &= (-0.32928, 0.0500556, -0.928716), \\ g_0 &= (0.124423, -0.105239, 0).\end{aligned}\tag{3.9}$$

It follows that the unstable line at q_0 is generated by e_0 while the stable plane π_0 is generated by $\{f_0, g_0\}$. Let N_1 be the intersection of the plane $\bar{x} = 1$ and the unstable line at q_0 . Thus $N_1 = (1, 0.118229, 0.96585)$. Let $X(\tau) = (\bar{x}(\tau), \bar{y}(\tau), \bar{z}(\tau))$ be the solution of (3.5) in the region III with the initial condition N_1 . If $\tau = 8.2870398$ then $N_2 = X(8.2870398) = (1, -0.249007, 2.42616)$ belongs to intersection of the plane $\bar{x} = 1$ and the stable plane π_0 since $\det[N_2, f_0, g_0] = 0$. Therefore a homoclinic loop at q_0 can be defined by the trajectory along the unstable eigenvector e_0 . By symmetry of (3.5), there is another homoclinic loop at q_0 defined by the trajectory of the unstable eigenvector $-e_0$.

The chaotic nature of the Chua's (1.1) was proved by establishing the existence of a homoclinic loop of the saddle focus at the origin and by applying the Shil'nikov condition

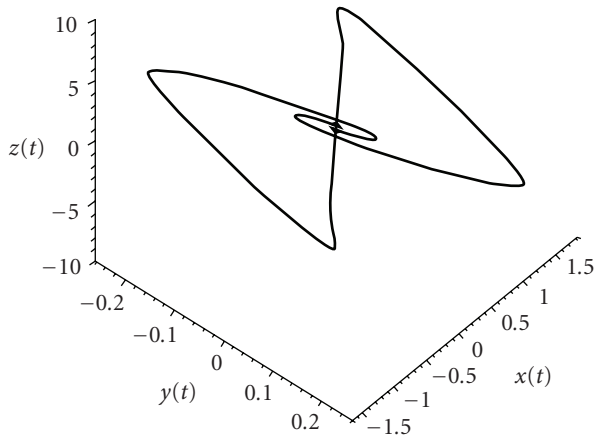


Figure 3.1. Homoclinic loops. They were obtained solving (3.5) with initial conditions $N_1 = (1, 0.118229, 0.96585)$ and $M_1 = (-1, -0.118229, -0.96585)$ and $\tau \in [-10, 30]$.

$\lambda_{00} > -\text{Re}(\lambda_{01}) > 0$ [11]. In this work, Shil'nikov saddle-focus condition is satisfied by $1334.94\Omega \leq R \leq 2000\Omega$. Figure 3.1 presents a draft of the homoclinic loop found at $\alpha = -1.64042$ corresponding to $R = 1490.46\Omega$.

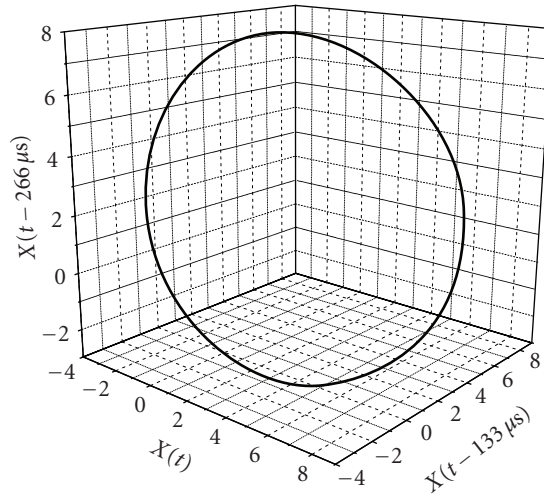
In Figure 3.1 it is possible to identify the stable and unstable manifolds associated with it. The value of R for the homoclinic loops is near of the value found for the experimental measurements of the cycle-one attractor obtained with $R = 1480\Omega$ as will be presented in the next section. It should be pointed out that the nominal values of capacitors and resistors used in this implementation were selected by measurements with digital multimeters which are subjected to experimental errors between 1% and 3%. Thus the value of R for the occurrence of the homoclinic loops is compatible with our experimental results.

4. Experimental results and discussion

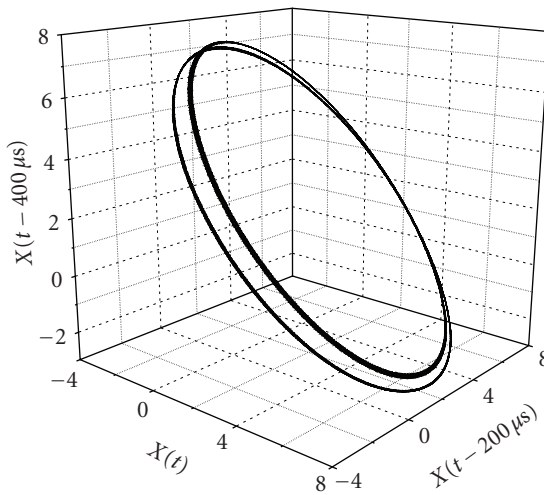
For this work we have carried out time series measurements of the variable $x(t)$ for some R values and proceeded as described in Section 2. Figures 4.1 and 4.2 present the four selected attractors obtained from time series with R as 1480Ω , 1560Ω , 1670Ω , and 1792Ω . They correspond to a cycle one, cycle two, chaotic-like in one region and the double scroll, respectively. For attractor reconstruction (see Figures 4.1 and 4.2) proper time delay [20] and the embedding dimension [21] were determined.

Figure 4.3 presents the mutual information for attractor 4. The first minimum corresponds to the optimal time delay for the delayed vectors. For the double scroll attractor it is of 7-time steps of $33\mu\text{s}$.

The false nearest neighbors algorithm was applied to verify if the time series is sensitive to noise [22]. Since Chua's system is a three-variable system, it turns out that false nearest neighbors should indicate the embedding dimensions as three. A higher than three embedding dimension for this system would mean significant noise contamination [17, 18].



(a) Attractor 1

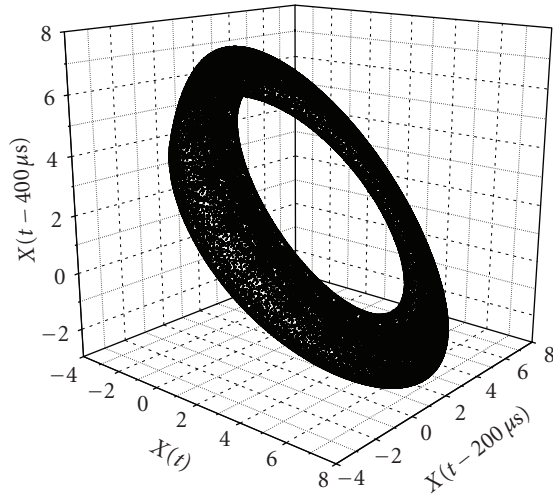


(b) Attractor 2

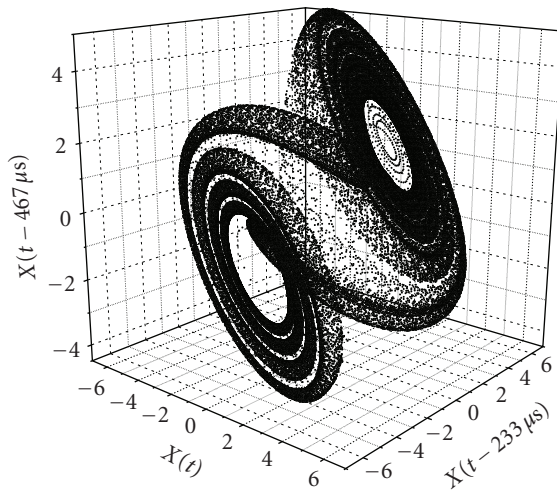
Figure 4.1. Periodic attractors obtained from delayed coordinates of the x variable. (a) Was obtained from a time series with $R = 1480\Omega$ and is a cycle one attractor. (b) Was obtained from a time series with $R = 1560\Omega$ and is a cycle two attractor.

Since our results indicate no false nearest neighbors for embedding dimensions above 3, we can neglect noise contribution for the geometric invariants that will be presented in the following.

Figure 4.4 presents the false nearest neighbor plot for attractor 4. As can be seen, the proper embedding dimension is 3. In Figure 4.5, we present the Poincaré section for the



(a) Attractor 3



(b) Attractor 4

Figure 4.2. Chaotic attractors obtained from delayed coordinates of the x variable. (a) Was obtained from a time series with $R = 1670\Omega$ and occupies one state space region. (b) Was obtained from a time series with $R = 1792\Omega$ and is the double scroll attractor.

periodic attractors presented in Figure 4.1. In Figure 4.5(a) we have a fixed point obtained from attractor 1. In Figure 4.5(b) we have a period two pair of points obtained from attractor 2.

In Figure 4.6 we present the Poincaré section for the chaotic attractors presented in Figure 4.2. In Figure 4.6(a) we have the Poincaré section for attractor 3 represented by a

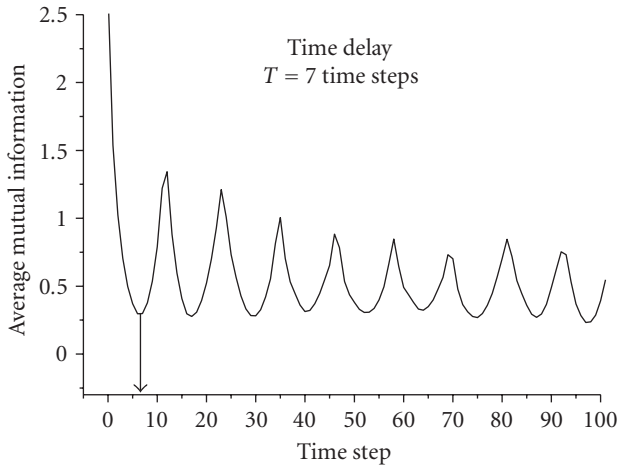


Figure 4.3. Average mutual information for the attractor 4. The first minimum corresponds to the optimal time delay.

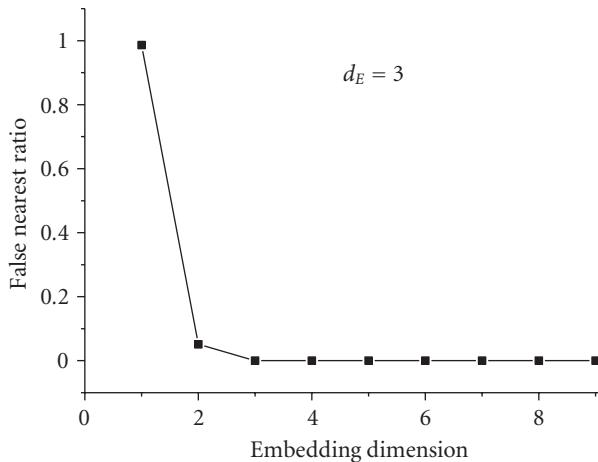
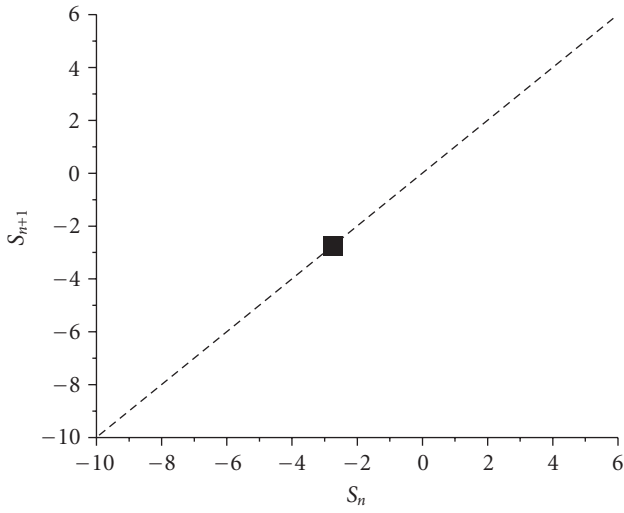


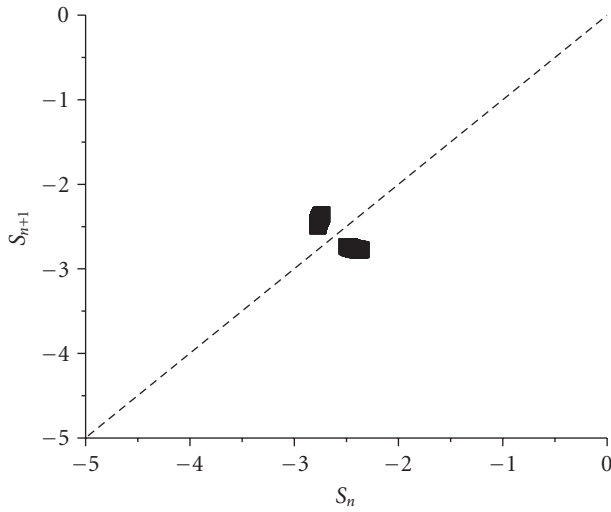
Figure 4.4. False nearest neighbor ratio as a function of the embedding dimension. The false nearest neighbors become negligible after $d_E = 3$. This confirms that the Chua's circuit is a 3-variable system.

continuous curve crossing the $y = x$ line. In Figure 4.6(b) we have a more complex pattern obtained for attractor 4. It is basically composed by two curves, one corresponding to each side of the “scroll” of the flow attractor.

Time series analyses were carried for all attractors. The estimated parameters were the Lyapunov spectrum [23] with its subproduct the Kaplan-Yorke dimension (D_{KY}) [24] and the information dimension (D_1) [25]. D_1 was measured for both flow and map representations. We will present detailed analysis for attractor 4 and summarize the information for all attractors in a table that will follow.



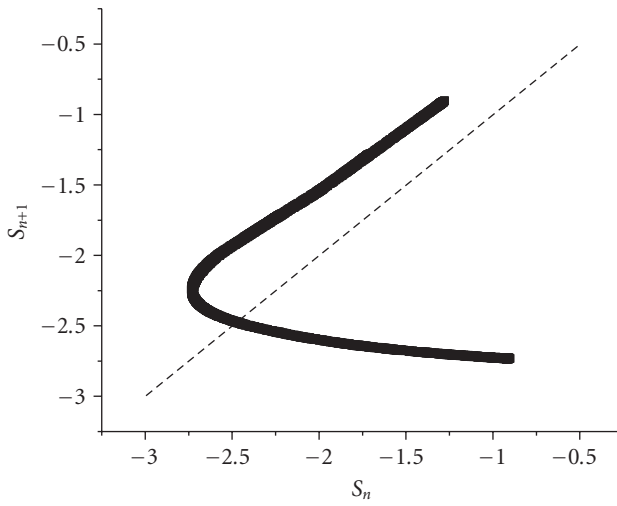
(a)



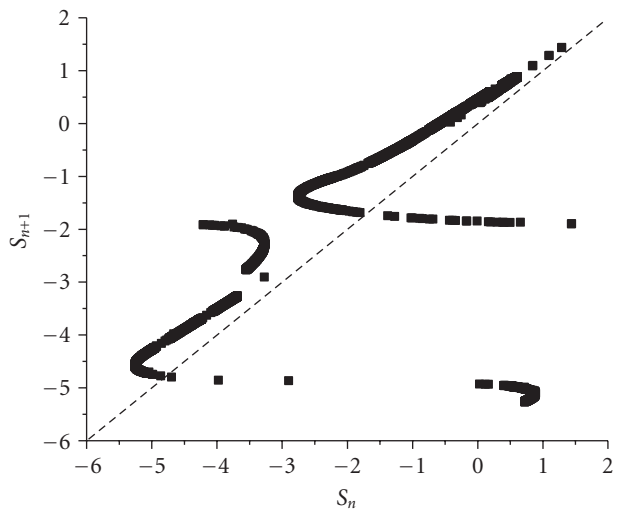
(b)

Figure 4.5. Poincaré section obtained from the extrema sequence of the attractors 1(a) and 2(b) presented in Figure 4.1. The dashed line is $y = x$, which shows that in (a) we have a fixed point and in (b) a period 2 points.

Figure 4.7 presents the Lyapunov spectrum for the attractor 4, obtained by using the method described in [23] and implemented in [17, 18]. It is characterized by a positive, a null, and a negative Lyapunov exponent. This configuration is a characteristic of chaotic attractors. The Kaplan-Yorke dimension for this attractor is evaluated as $D_{KY} = 2.14$.



(a)



(b)

Figure 4.6. Poincaré section obtained from the extrema sequence of the attractors 3(a) and 4(b) presented in Figure 4.3. The dashed line is $y = x$, which shows that in both cases the attractors resemble chaotic.

Dimension analysis gives complementary information since it is common to find strange attractors with fractal shape.

D_{KY} is considered as equivalent to D_1 [26]. Considering this we present in Figure 4.8 the D_1 for attractor 4. In Figure 4.8(a) we present the results for the D_1 measured for the flow attractor and in Figure 4.8(b) for its Poincaré map. D_1 is characterized by a region

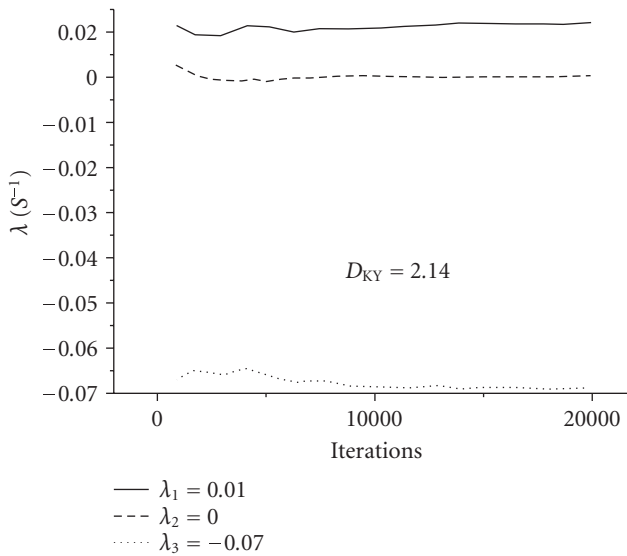


Figure 4.7. Lyapunov spectrum for attractor 4. Each Lyapunov exponent corresponds to a state space direction. The positive Lyapunov exponent is an evidence of chaotic behavior. D_{KY} is evaluated as $D_{KY} = 2.14$.

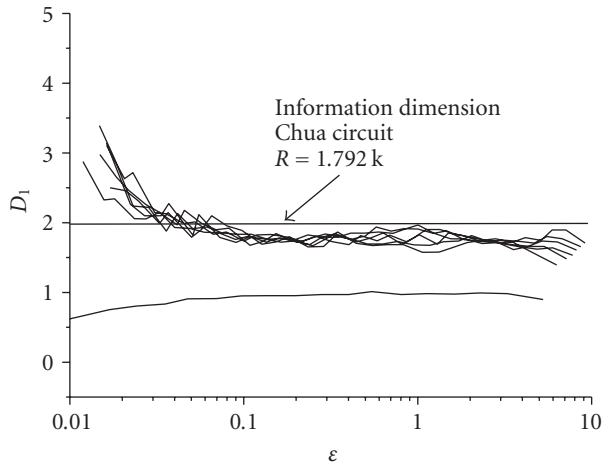
of zero slope independent of the embedding dimensions above the proper one (i.e., 3 for Chua's circuit). In Figure 4.8(a) D_1 is estimated as 1.8 ± 0.1 and in Figure 4.8(b) 1.2 ± 0.1 .

According to [26] the dimension of a map attractor is related to the dimension of its flow attractor by a difference of one unity. This occurs because the map is obtained by eliminating the flow direction which is related to the null Lyapunov exponent. Since the null Lyapunov exponent is associated to a dimension of one, the map information dimension (D_{1M}) must be related to the flow information dimension (D_{1F}) by $D_{1M} = D_{1F} - 1$.

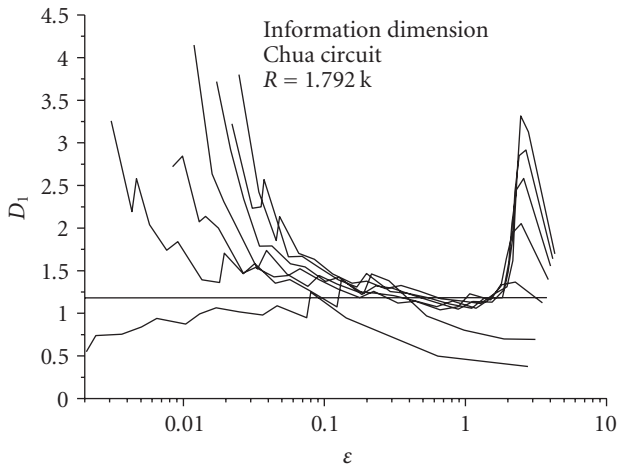
Considering that $D_{KY} \sim D_{1F}$ we can infer that our measurements of D_{1F} are underestimated and that $D_{1M} + 1$ is compatible with the corresponding values of D_{KY} . The reason for the low value of D_{1F} is yet unknown but certainly it is related to the direction of the flow and thus to the null Lyapunov exponent.

Table 4.1 summarizes the results for the four presented attractors. The first column, assigned as #, indicates the number of the attractor as defined in the text. 1, 2, 3, and 4 correspond to the attractors obtained with R in ohms defined in column 2. The third column is D_{1M} , measured for the Poincaré maps and the fourth column presents D_{1F} , measured for the flow attractor. The fifth column is the Kaplan-Yorke dimension. The sixth column is the minimal embedding dimension obtained from the false nearest neighbor algorithm. The last column lists the three Lyapunov exponents in decreasing order.

Both periodic attractors presented three negative Lyapunov exponents, but the first two can be considered as null when compared with the third value. Considering this,



(a)



(b)

Figure 4.8. Information dimension D_1 for attractor 4. In (a) we present the result for the flow attractor and in (b) for its Poincaré map. In (a) the straight line is a guide that indicates that the dimension is below 2.0. In (b) the dimension is evaluated at 1.2.

D_{KY} is estimated as 1.0 for attractors 1 and 2. This is in agreement with the value of 1.0 obtained for D_{IF} .

Attractors 3 and 4 presented one positive, one null, and one negative Lyapunov exponent. The sum of the exponents is negative, which means that attractors contract volume in state space. The Kaplan-Yorke dimension for them is above 2.0, whilst the D_1 was determined as 1.8 for the flow representation of the attractors.

Table 4.1. Analysis results for the four presented attractors.

#	$R\Omega$	D_{1M}	D_{1F}	D_{KY}	FNN	Lyap. Exp.
1	1480	0.0	1.0	1.0	2	-0.01
						-0.02
						-0.15
2	1560	0.0	1.0	1.0	3	-0.02
						-0.02
						-0.15
3	1670	1.3	1.8	2.19	3	0.01
						0.00
						-0.08
4	1792	1.2	1.8	2.14	3	0.01
						0.00
						-0.07

As discussed above the latter value is underestimated. Two facts corroborate for this assumption. One is that D_1 measured for the Poincaré maps of the attractors does not differ by one unity from the measurement carried on the flow attractors, but they do differ by approximately one unity from the Kaplan-Yorke dimension.

The other fact is also related to the Poincaré map of the attractors. The visual inspection of the Poincaré maps presented in Figure 4.6 indicates that they are objects with dimension greater than 1. Thus, the flow attractor must be an object with a dimension greater than 2, since by adding 1 to a number between 1 and 2 the resulting number must be between 2 and 3.

5. Summary

We have implemented experimentally an operational amplifier inductorless realization of the Chua's circuit.

A homoclinic loop was found by numerical analysis of normalized Chua's differential equations at a parameter corresponding to $R = 1490.46\Omega$. Indeed, bifurcations were observed experimentally in the vicinity of R for the homoclinic loop.

We selected four representative attractors obtained with R as 1480Ω , 1560Ω , 1670Ω , and 1792Ω to present in this work. They correspond to a cycle one, cycle two, chaotic-like in one region, and the double scroll, respectively.

Considering the double scroll, that is, for $R = 1792\Omega$, the information dimension of a three-dimensional delay vector reconstruction of the attractor (D_{1F}) and of its Poincaré map (D_{1M}) are 1.8 and 1.2, respectively. Also the Lyapunov spectrum gives positive, null, and negative exponents with a Kaplan-Yorke dimension as 2.14 characterizing the attractor as chaotic. This indicates that the flow attractor dimension has been underestimated and that the Kaplan-Yorke dimension is better suited for this attractor.

Acknowledgments

The authors acknowledge the Brazilian Agencies CNPq, CAPES, and FAPEMIG for financial support. R. M. Rubinger and L. F. Mello are partially supported by FAPEMIG, under the projects EDT 1968/03 and EDT 1929/03, respectively.

References

- [1] L. O. Chua, "Chua's circuit: ten years later," *IEICE Transactions on Fundamentals of Electronics, Communications and Computer Sciences*, vol. E77-A, no. 11, pp. 1811–1822, 1994.
- [2] G.-P. Jiang, W. K.-S. Tang, and G. Chen, "A simple global synchronization criterion for coupled chaotic systems," *Chaos, Solitons and Fractals*, vol. 15, no. 5, pp. 925–935, 2003.
- [3] J. Zhang, C. Li, H. Zhang, and J. Yu, "Chaos synchronization using single variable feedback based on backstepping method," *Chaos, Solitons and Fractals*, vol. 21, no. 5, pp. 1183–1193, 2004.
- [4] M. T. Yassen, "Adaptive control and synchronization of a modified Chua's circuit system," *Applied Mathematics and Computation*, vol. 135, no. 1, pp. 113–128, 2003.
- [5] T. Wu and M.-S. Chen, "Chaos control of the modified Chua's circuit system," *Physica D: Nonlinear Phenomena*, vol. 164, no. 1-2, pp. 53–58, 2002.
- [6] C.-C. Hwang, H.-Y. Chow, and Y.-K. Wang, "A new feedback control of a modified Chua's circuit system," *Physica D: Nonlinear Phenomena*, vol. 92, no. 1-2, pp. 95–100, 1996.
- [7] K. Li, Y. C. Soh, and Z. G. Li, "Chaotic cryptosystem with high sensitivity to parameter mismatch," *IEEE Transactions on Circuits and Systems I*, vol. 50, no. 4, pp. 579–583, 2003.
- [8] Z. Li, K. Li, C. Wen, and Y. C. Soh, "A new chaotic secure communication system," *IEEE Transactions on Communications*, vol. 51, no. 8, pp. 1306–1312, 2003.
- [9] E. P. dos Santos, M. S. Baptista, and I. L. Caldas, "Dealing with final state sensitivity for synchronous communication," *Physica A: Statistical Mechanics and Its Applications*, vol. 308, no. 1–4, pp. 101–112, 2002.
- [10] L. O. Chua, "Chua's circuit: an overview ten years later," *Journal of Circuits Systems and Computers*, vol. 4, no. 2, pp. 117–159, 1994.
- [11] L. P. Shil'nikov, "Chua's circuit: rigorous results and future problems," *IEEE Transactions on Circuits and Systems I*, vol. 40, no. 10, pp. 784–786, 1993.
- [12] C. Letellier, G. Gouesbet, and N. F. Rulkov, "Topological analysis of chaos in equivariant electronic circuits," *International Journal of Bifurcation and Chaos in Applied Sciences and Engineering*, vol. 6, no. 12B, pp. 2531–2555, 1996.
- [13] D. M. Maranhão and C. P. C. Prado, "Evolution of chaos in the Matsumoto-Chua circuit: a symbolic dynamics approach," *Brazilian Journal of Physics*, vol. 35, no. 1, pp. 162–169, 2005.
- [14] S. Kahan and A. C. Sicardi-Schifino, "Homoclinic bifurcations in Chua's circuit," *Physica A: Statistical Mechanics and Its Applications*, vol. 262, no. 1-2, pp. 144–152, 1999.
- [15] T. Matsumoto, L. O. Chua, and K. Ayaki, "Reality of chaos in the double scroll circuit: a computer-assisted proof," *IEEE Transactions on Circuits and Systems*, vol. 35, no. 7, pp. 909–925, 1988.
- [16] L. A. B. Tôrres and L. A. Aguirre, "Inductorless Chua's circuit," *Electronics Letters*, vol. 36, no. 23, pp. 1915–1916, 2000.
- [17] <http://www.mpipks-dresden.mpg.de/~tisean/>.
- [18] H. Kantz and T. Schreiber, *Nonlinear Time Series Analysis*, Cambridge University Press, Cambridge, UK, 1997.
- [19] A. F. Gribov and A. P. Krishchenko, "Analytical conditions for the existence of a homoclinic loop in Chua circuits," *Computational Mathematics and Modeling*, vol. 13, no. 1, pp. 75–80, 2002.

- [20] A. M. Fraser and H. L. Swinney, "Independent coordinates for strange attractors from mutual information," *Physical Review A*, vol. 33, no. 2, pp. 1134–1140, 1986.
- [21] M. B. Kennel, R. Brown, and H. D. I. Abarbanel, "Determining embedding dimension for phase-space reconstruction using a geometrical construction," *Physical Review A*, vol. 45, no. 6, pp. 3403–3411, 1992.
- [22] T. Wu and M.-S. Chen, "Chaos control of the modified Chua's circuit system," *Physica D: Non-linear Phenomena*, vol. 164, no. 1-2, pp. 53–58, 2002.
- [23] M. Sano and Y. Sawada, "Measurement of the Lyapunov spectrum from a chaotic time series," *Physical Review Letters*, vol. 55, no. 10, pp. 1082–1085, 1985.
- [24] J. Kaplan and J. Yorke, "Chaotic behavior of multidimensional difference equations," in *Functional Differential Equations and Approximation of Fixed Points*, H. O. Peitgen and H. O. Walther, Eds., Springer, New York, NY, USA, 1987.
- [25] R. Radii and A. Politi, "Statistical description of chaotic attractors: the dimension function," *Journal of Statistical Physics*, vol. 40, no. 5-6, pp. 725–750, 1985.
- [26] J. P. Eckmann and D. Ruelle, "Ergodic theory of chaos and strange attractors," *Reviews of Modern Physics*, vol. 57, no. 3, pp. 617–656, 1985.

R. M. Rubinger: Instituto de Ciências Exatas, Universidade Federal de Itajubá,
37500-903 Itajubá, MG, Brazil
Email address: rero@unifei.edu.br

A. W. M. Nascimento: Instituto de Ciências Exatas, Universidade Federal de Itajubá,
37500-903 Itajubá, MG, Brazil
Email address: valdisejnsantos@uol.com.br

L. F. Mello: Instituto de Ciências Exatas, Universidade Federal de Itajubá,
37500-903 Itajubá, MG, Brazil
Email address: lfmelo@unifei.edu.br

C. P. L. Rubinger: Instituto de Ciências Exatas, Universidade Federal de Itajubá,
37500-903 Itajubá, MG, Brazil
Email address: carla@fis.ua.pt

N. Manzaneres Filho: Instituto de Engenharia Mecânica, Universidade Federal de Itajubá,
37500-903 Itajubá, MG, Brazil
Email address: nelson@unifei.edu.br

H. A. Albuquerque: Departamento de Física, Centro de Ciências Tecnológicas,
Universidade do Estado de Santa Catarina, 89223-100 Joinville, SC, Brazil
Email address: dfi2haa@joinville.udesc.br



Hindawi

Submit your manuscripts at
<http://www.hindawi.com>

